



Observing bursting and chirping coherence modes in plasma of solely electron cyclotron wave heating

Mingyuan Wang^{1,2}, Jixing Yang^{1,2,†}, Yuejiang Shi^{3,4,†}, Jiaqi Dong^{3,4},
Wenjun Liu^{3,4}, Hongyue Li^{3,4}, Yingying Li^{3,4}, Jie Wu⁵, Ad Liu⁵, Ge Zhuang⁵,
Yahui Wang^{1,2}, Ruibo Zhang^{1,2}, Baoshan Yuan^{3,4}, Y.-K. Martin Peng^{3,4}
and EXL-50 team

¹School of Mathematics and Physics, Anqing Normal University, Anqing 246133, PR China

²International Joint Research Center of Simulation and Control for Population Ecology of Yangtze River
in Anhui, Anqing, Anhui 246133, PR China

³Hebei Key Laboratory of Compact Fusion, Langfang 065001, PR China

⁴ENN Science and Technology Development Co., Ltd., Langfang 065001, PR China

⁵University of Science and Technology of China, Hefei 230026, PR China

(Received 21 January 2024; revised 18 June 2024; accepted 25 June 2024)

This study presents observations of coherent modes (CMs) in a spherical tokamak using a microwave interferometer near the midplane. The CMs within the 30–60 kHz frequency range were observed during electron cyclotron resonance heating only, and the frequency of the CMs increased proportionally with the square root of the electron temperature near $R = 0.7m$. Generally, these modes displayed bursting and chirping signatures with strong density rise and fall. Their appearance indicated an increase in the intensity of hard x rays, suggesting a deterioration in energetic electron confinement. Furthermore, the effect of CMs on the intensity of energetic electron-driven whistler waves was observed. They decreased when CMs were present and gradually increased with the decrease in CM intensity. The CMs may influence the intensity of whistler waves by affecting the energetic electron confinement.

Keywords: plasma waves, plasma nonlinear phenomena, plasma instabilities

1. Introduction

Instabilities are an essential phenomenon in magnetic fusion confinement research, encompassing electromagnetic and electrostatic instabilities (Burrell 1997; Terry 2000; Kennedy 2023). Instabilities in the ion acoustic range are significant because they affect plasma confinement and energy transport properties (Burrell 1997).

Geodesic acoustic modes (GAMs) (Conway, Smolyakov & Ido 2021) are the most common type of electrostatic instability in magnetic confinement fusion plasma where the frequency is positively correlated with the plasma sound velocity ($c_s = \sqrt{\gamma(T_e + T_i)/m_i}$). Here, T_e and T_i are the electron and ion temperatures, respectively, and m_i is the ion mass.

† Email addresses for correspondence: yangjx@mail.ustc.edu.cn, yjshi@ipp.ac.cn

The GAM, a prevalent oscillatory flow phenomenon in toroidal magnetic confinement fusion devices, is supported by plasma compressibility resulting from toroidal geodesic curvature. These oscillations manifest perpendicular flow with $m = 0$, density modulation with $m = \pm 1 \sin \theta$ and magnetic halo $B_\theta = \sin 2\theta$, characterized by a frequency of $\omega_{\text{GAM}}^2 = 2c_s^2/R_0^2(1 + 1/2q^2)$, where R_0 is the toroidal major radius and q is the local safety factor. It should be noted that the ion-acoustic waves (IAWs) are also an electrostatic instability whose frequency is positively correlated with c_s . They have not received much attention in tokamaks because of their small effect on plasma turbulence. If the electron temperature is greater than the ion temperature, the phase velocity of the wave is much greater than the thermal velocity of the ions, and the ion contribution to Landau damping diminishes.

The interaction between energetic electrons and plasma can induce beta induced Alfvén eigenmodes (BAE) with frequencies near the GAM (Zonca, Chen & Santoro 1996; Chen *et al.* 2011; Heidbrink *et al.* 2020), posing a significant challenge for fusion device development (Bierwage, Aiba & Shinohara 2015; Kolmes, Ochs & Fisch 2022). A theoretical consensus reveals a gap in the Alfvén continuum associated with beta and the geodesic curvature, with an accumulation point at its peak frequency coinciding with the GAM but showing Alfvén polarization. The low-frequency mode (LFM) is an interchange-like electromagnetic mode excited by a non-resonant drive of pressure gradients (Ma *et al.* 2023); the mode frequency is less than ω_{GAM} and close to the ion diamagnetic frequency ($\omega_{*\text{pi}}$). The LFM has low-frequency Alfvén modes, which are almost always undetectable on magnetic diagnostic instruments.

Therefore, understanding the physics of fluctuations in the GAM frequency range in plasma with $T_e/T_i > 1$ is crucial for further progress in fusion energy (Kolmes *et al.* 2022). In this study, we investigated the impact of coherent modes (CMs) in the GAM range on energetic electron transport in the EXL-50 tokamak. During experiments using electron cyclotron resonance heating (ECRH), bursting and chirping CMs were detected using a microwave interferometer (Li *et al.* 2021). Notably, the frequency of these CMs is directly proportional to the square root of the electron temperature (T_e). The fluctuations correspond to an increase in fast electron-loss radiation, affecting energetic electron loss. Investigations have also revealed a competitive relationship between CMs and whistler waves (Wang *et al.* 2023d, 2024), wherein CMs reduce the whistler wave intensity. Although no modulation of whistler waves by CMs has been observed, CMs conditionally reduce the whistler wave intensity by limiting the confinement of energetic electrons. The experimental results obtained from EXL-50 provide insights into the behaviour of plasma instabilities and their coupling to whistler waves. These findings help us understand wave-particle interactions and the effects of energetic electrons on plasma stability and confinement.

The remainder of this paper is organized as follows: § 2 describes the EXL-50 and high-frequency magnetic probes; § 3 presents the experimental results; § 4 presents the conclusions and discussion.

2. The EXL-50 tokamak

The EXL-50 is a medium-sized, spherical tokamak without a central solenoid. It has major and minor radii of approximately 0.58 and 0.41 m, respectively. The toroidal magnetic field strength (B_T) at a radius of approximately 0.58 m is approximately 0.48 T, while the aspect ratio (A) is greater than or equal to 1.45. The EXL-50 is primarily a hydrogen discharge, and the main plasma ions are hydrogen ions with small amounts of impurity ions such as boron and helium. The highest plasma current recorded in an experiment is 150 kA (Shi *et al.* 2022). The line integral electron density ranges

from $2 - 18 \times 10^{17} m^{-2}$. The plasma is heated using an electron cyclotron wave (ECW) at approximately 140 kilowatts (kW). The EXL-50 employs two sets of 28 GHz ECW systems operating in the O-mode to heat the plasma and drive the plasma current. System #1, with a gyrotron source power of 50 kW, is used to produce the initial plasma and form a closed flux surface. System #2, with a gyrotron source power of 400 kW, sustains the plasma current during the flattop phase for several seconds.

The plasma density and fluctuations have been determined using a microwave interferometer near the midplane (Li *et al.* 2021). This system measures the phase shift between two probing beams induced by the line-integrated plasma density. Density fluctuations are detected in the phase fluctuations of the signals. Localized electron temperature and density measurements are conducted using Thomson scattering (TS) (Li *et al.* 2022b). The Bremsstrahlung emission generated by energetic electron losses to the wall is measured using hard x ray (HXR) detectors (Cheng *et al.* 2021). The rise and fall in the low-frequency magnetic field (1–200 kHz) are measured using a magnetic probe. High-frequency magnetic probes are used to detect coherent electromagnetic fluctuations such as whistler waves (Wang *et al.* 2023b). The ECW heating generates an energetic electron population through stochastic heating (Wang *et al.* 2023c). These energetic electrons can provide free energy for the instabilities (Wang *et al.* 2023d, 2024).

3. Experimental results

Figure 1 illustrates the typical plasma discharge in the EXL-50 device, wherein CMs are observed. The temporal evolutions of the plasma current and density of two discharges, #9193 (black) and #19737 (blue), are shown in **figures 1(a)** and **1(b)**, respectively. **Figure 1(c)** shows the temporal evolution of the core electron and ion temperature for discharge #19737, during which the ECW is injected at approximately 200 kW in the O-mode. Here, the temperature of the bulk electrons exceeds that of the ions. Burst-like density fluctuations with chirping frequencies were observed using a microwave interferometer at specific time intervals of 2.8–3.5 and 1.8–3 s in shots #9193 and #19737, respectively. The level of density fluctuations ($\delta n_{CM}/n_{el}$) is between 0.1 % and 1 %. Moreover, the mean fluctuation frequency decreases as the electron temperature decreases.

We conducted an extensive analysis using data from more than 10 discharges to determine the relationship between the electron temperature and frequency of the mode. We observed a positive correlation between the frequency of the CM and electron temperature measured using the TS diagnostics at approximately 0.7 m from the centre of the plasma, as shown in **figure 2**. The frequency range of the fluctuations is comparable to frequency called CMs. Note that the TS is designed for a minimum density measurement of approximately $1 \times 10^{18} m^{-3}$, and the temperature error of the TS measurement is large at low densities ($< 1 \times 10^{18} m^{-3}$). The CMs frequency usually increases and then decreases during a burst cycle, and the CMs frequency chirping maintenance time in the experiment is usually more than 10 ms, which is much larger than the frequency chirping caused by the phase space variation.

As shown in **figure 3**, the presence of CMs increases HXR intensity. This represents a degradation in the energetic electron confinement, as HXR intensity refers to the thick-target radiation caused by energetic electrons hitting the device wall. Therefore, CMs may lead to an increase in the loss of energetic electrons. Moreover, when energetic electrons hit the device wall, wall outgassing occurs, which increases the background plasma density and the electron collision rate. With a further increase in the background electron density as well as in the loss of energetic electrons, the free energy supporting the CM may decrease, and the frequency and intensity of the CM may decrease and eventually

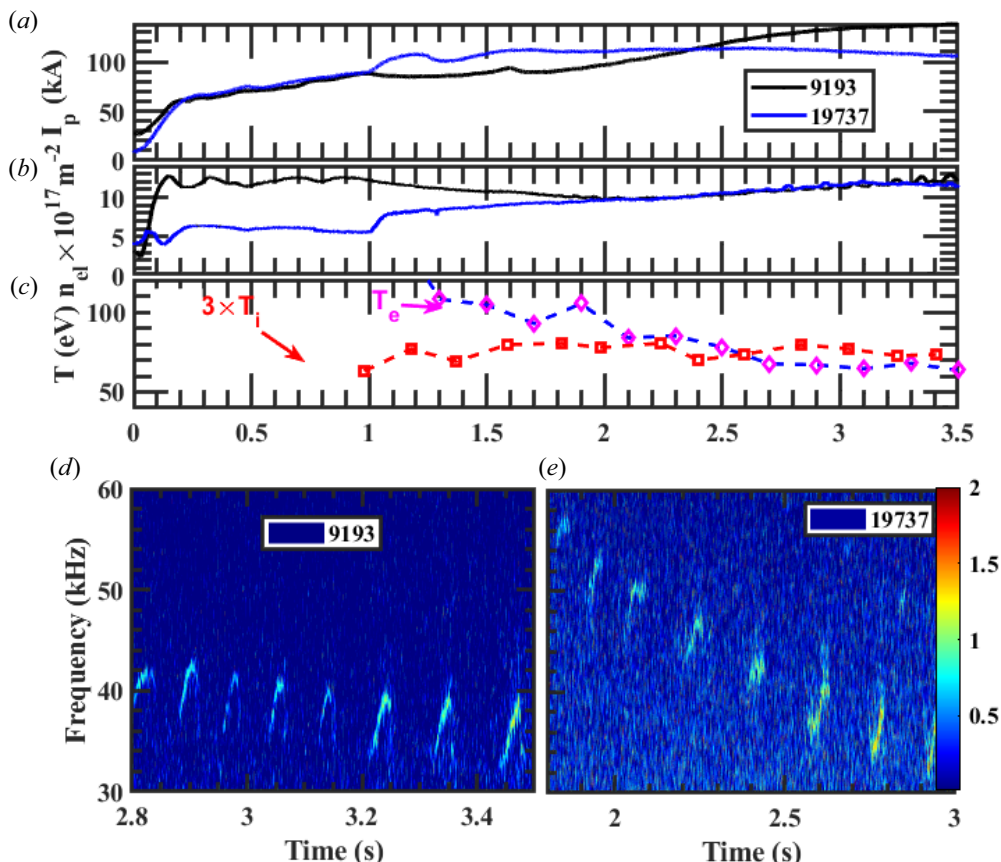


FIGURE 1. Typical observations of CMs in EXL-50 plasma discharges. Panels (a) and (b) show the temporal evolution of the plasma current and line-averaged density, respectively, for two discharges: #9193 (black) and #19737 (blue). Panel (c) shows the time evolution of core electrons and ion temperatures (ion temperature multiplied by three) during discharge #19737. Panels (d) and (e) show the power spectra of plasma density fluctuations exhibiting burst CMs in the ion acoustic frequency range (10–100 kHz) for discharges #9193 and #19737.

disappear. Once a certain level of parameter accumulation is reached, a new cycle of CM excitation begins.

Energetic electrons can initiate whistler waves (Spong *et al.* 2018; Wang *et al.* 2024). Theoretical predictions suggest interactions between low-frequency instabilities and whistler waves via wave–particle or wave–wave interactions. In shot #14 954, whistler waves and CMs were simultaneously observed (figure 4). The CMs were observed at 2.25 and 2.45 s. The presence of CMs was associated with a decrease in the frequency and intensity of the whistler wave, suggesting possible interactions between them.

Figure 5 shows the temporal evolution of plasma density, density fluctuation intensity of CMs and whistler wave magnetic field fluctuations for over 2.2 to 2.5 s. When the CMs emerge, the plasma density increases, whereas the whistler wave intensity decreases. Figure 5(d) shows the correlation between the intensity of the CMs and fluctuations in the whistler wave magnetic field. Here, the intensity of the CMs increases before that of the whistler waves. Although a slight decrease in the plasma density is observed at approximately 2.35 s, the whistler wave intensity does not exhibit a considerable decrease.

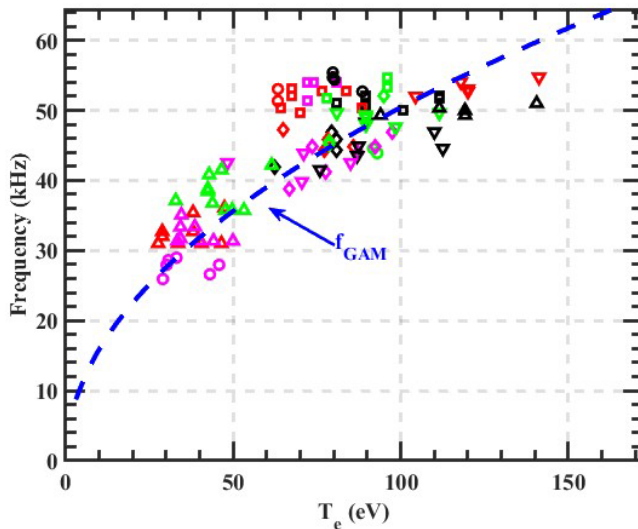


FIGURE 2. Correlation between the frequency of CMs and electron temperature. The scatter plot shows the electron temperature measured using TS at approximately 0.7 m on the horizontal axis versus the frequency of CMs on the vertical axis. Here, a positive correlation is observed, with the mode frequency increasing with an increase in the electron temperature.

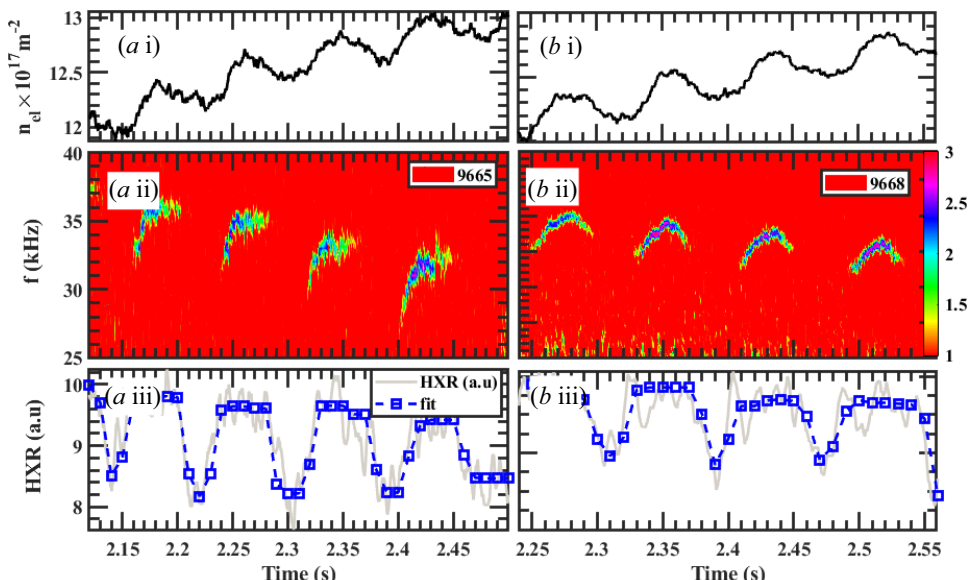


FIGURE 3. Time evolution of line-averaged density (a i and b i), the rise and fall in the power spectra (a ii and b ii) of the CMs and HXR intensity over time (a iii and b iii), including the fitted curve represented by the blue dashed line (a iii and b iii). The HXR signal shows a considerable increase when CMs appear (represented by blue) and a decrease as the modes dissipate. This indicates a greater energetic electron loss from the plasma during CM driving.

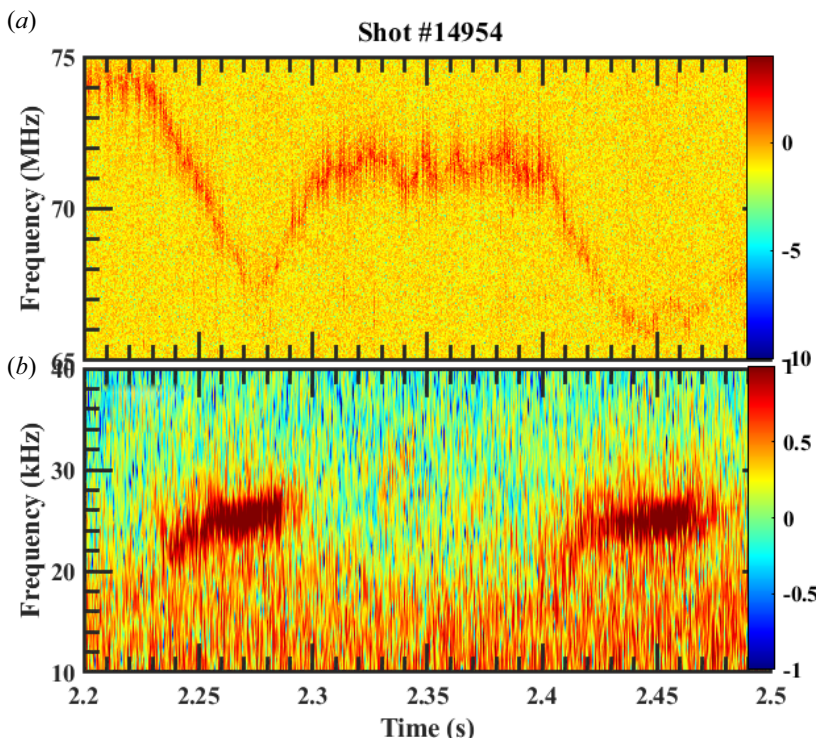


FIGURE 4. Observation of CMs and whistler waves in EXL-50 discharge. Panel (a) shows the power spectra of high-frequency magnetic fluctuations exhibiting whistler wave signals, and (b) shows the power spectra of plasma density fluctuation signals. The concurrent detection of CMs and whistler activity in their respective frequency ranges is evident. An inverse correlation between the density fluctuation intensity of CMs and whistler wave magnetic fluctuation intensity suggests a competitive relationship.

This implies that the effect of density change on the whistler wave intensity is relatively weak. Hence, the impact of density changes on the CMs and whistler wave intensity can be disregarded in this procedure, while the depletion of energetic electrons may be responsible for reducing the whistler wave intensity.

3.1. Discussion

Owing to the limitations imposed by the diagnosis, it is currently difficult to identify the type of instability in question. Nevertheless, existing theories can facilitate pertinent discussions regarding the probability of IAW, GAM and BAE.

The EXL-50 generally uses only an ECW to heat and drive the plasma current, which is transported by energetic electrons. The drift velocity of the bulk electrons ($5 \times 10^4 \text{ m s}^{-1}$) is lower than the ion acoustic velocity ($\sim 10^5 \text{ m s}^{-1}$). Consequently, the IAW is difficult to stimulate under current conditions (Lesur, Diamond & Kosuga 2014). Although the frequency of the CM is consistent with the dispersion relation of the GAM, according to the theory of GAMs, the GAM has a density fluctuation component with $m=1$, whose fluctuation strength near the midplane is small (Conway *et al.* 2021). The EXL-50 microwave interferometer is closeted near the midplane of the device, and strong density fluctuations (0.1 %–1 %) have been measured. Therefore, the CM is unlikely to be GAM.

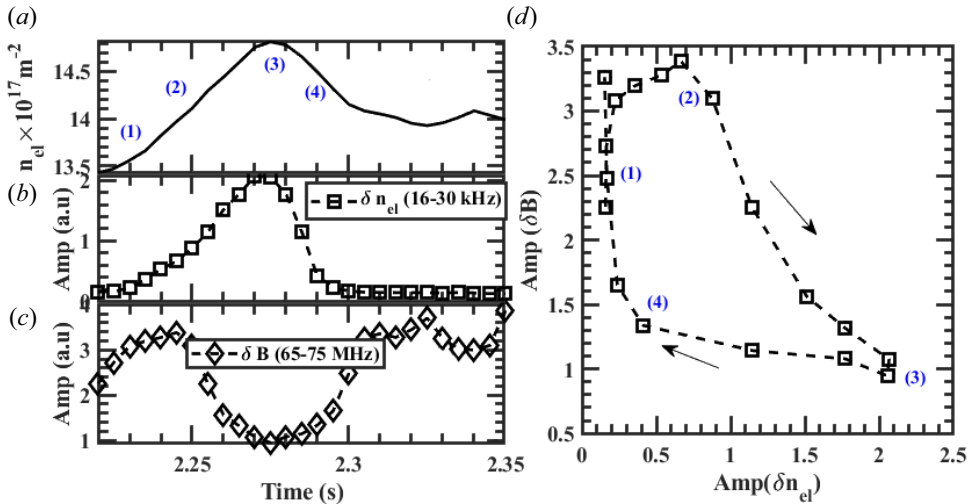


FIGURE 5. Time evolution of: (a) line-averaged plasma density; (b) CM density fluctuation; and (c) whistler wave magnetic field fluctuation over time in an EXL-50 discharge. Following the appearance of CMs, the plasma density increases while the whistler wave intensity decreases. Panel (d) shows the relationship between the intensity of the CM and whistler wave magnetic fluctuation (with four time points), wherein the CM intensity rises before the whistler wave intensity does.

Note that BAE has a GAM-like dispersion relationship (Heidbrink *et al.* 2020). However, no significant CM magnetic field rise and fall components were observed in the EXL-50 experiment. Although both LFM and BAE were observed in the DIII-D experiment, the magnetic field fluctuation component of LFM was also not observed (Heidbrink *et al.* 2020). This suggests that the electromagnetic rise and fall are not necessarily measured by the magnetic probe. This could be due to (i) the relatively local mode structure, (ii) the weak fluctuation intensity and (iii) the cutoff of the fluctuation that propagates from the core to the edge.

According to Zonca *et al.* (1996), for $\Omega_{\text{pi}}^2 \ll (\frac{7}{4} + \tau)q^2$, only the BAE accumulation point may be unstable when $\eta_i > \eta_{ic}$, and $\text{Im}(\Omega)$ increases linearly with η_i and Ω_{ni} , where $\eta_i = L_{\text{ni}}/L_{\text{ti}}$, $\tau = T_e/T_i$ and $\eta_{ic} \sim (2/\sqrt{7} + 4\tau)\omega_{ti}/q\omega_{\text{ni}}$. As shown in figure 1(c), $T_e/T_i \sim 3$ at $R = 0.7$ m. Assuming $R/L_{\text{ni}} \sim R/L_{\text{ne}} \sim 4$, $R/L_{\text{ti}} \sim R/L_{\text{te}} \sim 8$ (Wang *et al.* 2023a). Here η_{ic} and $\Omega_{\text{pi}}^2/(\frac{7}{4} + \tau)q^2$ are shown in figure 6; $\eta_i > \eta_{ic}$ and $\Omega_{\text{pi}}^2/(\frac{7}{4} + \tau)q^2 < 0.2$ with $q = 2$, $n = 4$, and the BAE accumulation point may be unstable on EXL-50.

3.2. Summary

In this study, we detected CMs on an EXL-50 spherical tokamak using microwave interferometry. We observed the modes during ECRH, wherein they exhibited bursting and frequency-chirping signatures.

The mode frequency increased with an increase in the electron temperature, and the mode had burst and chirp characteristics. The burst of CMs correlated with an increase in the HXR emission and electron density, implying the possible degradation of the energetic electron confinement. Energetic electrons hitting the walls of the device led to wall outgassing, which led to an increase in the background plasma density. A competitive relationship was also observed between CMs and whistler waves, with the

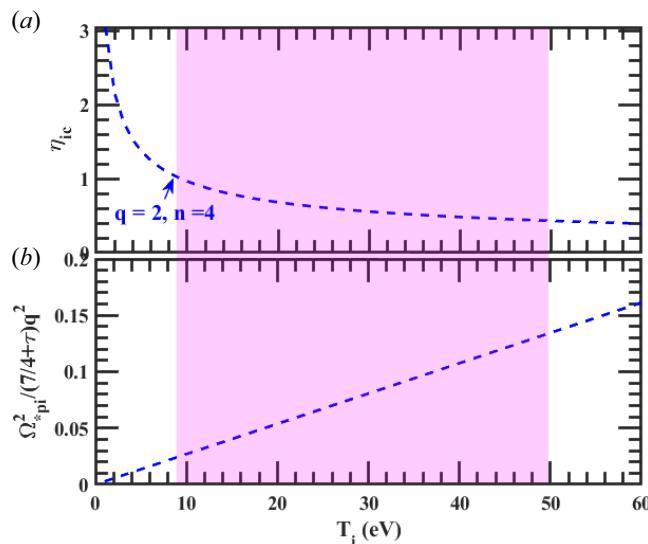


FIGURE 6. Here η_{ic} and $\Omega_{*pi}^2 / ((7/4 + \tau)q^2)$ versus T_i with $q = 2$ and $n = 4$. On EXL-50, typical T_i is between 20 and 50 eV, and the BAE accumulation point may be unstable.

former suppressing the intensity of the latter. The CM led to an increase in the loss of energetic electrons. We speculate that the suppression of whistlers by the CM is achieved by decreasing the number of energetic electrons. The CM frequency also had a chirping characteristic during a burst cycle, which usually increases and then decreases. This could be caused by the change in bulk plasma temperature. Although the source of the CM drive remains unknown, BAE is a potential candidate.

Acknowledgements

The authors thank R. Ma, W. Chen and W.X. Ding for their fruitful physical discussions.

Editor H. Zohm thanks the referees for their advice in evaluating this paper.

Funding

This work has been supported by the Natural Science Foundation of China (G.Z., grant number U1967206), Natural Science Research Project of Anhui Educational Committee (grant number 2024AH051100) and Fundamental Research Funds for the Central Universities (grant number WK3420000018).

Declaration of interests

The authors report no conflict of interest.

Data availability statement

The data that support the findings of this study are available upon reasonable request to the corresponding author.

REFERENCES

- BIERWAGE, A., AIBA, N. & SHINOHARA, K. 2015 Alfvén acoustic channel for ion energy in high-beta tokamak plasmas. *Phys. Rev. Lett.* **114** (1), 015002.

- BURRELL, K.H. 1997 Effects of $E \times B$ velocity shear and magnetic shear on turbulence and transport in magnetic confinement devices. *Phys. Plasmas* **4** (5), 1499–1518.
- CHEN, W., DING, X.T., LIU, Y., YANG, Q.W., JI, X.Q., YUAN, G.Y., ZHANG, Y.P., ISOBE, M., DONG, Y.B., HUANG, Y., ZHOU, J., ZHOU, Y., LI, W., FENG, B.B., SONG, X.M., DONG, J.Q., SHI, Z.B., DUAN, X.R., AND HL-2A TEAM 2011 Destabilization of beta-induced Alfvén eigenmodes in the HL-2A tokamak. *Nucl. Fusion* **51** (6), 063010.
- CHENG, S.K., ZHU, Y.B., CHEN, Z.Y., LI, Y.X., BAI, R.H., CHEN, B. & LIU, M.S. 2021 Tangential hard x-ray diagnostic array on the EXL-50 spherical tokamak. *Rev. Sci. Instrum.* **92** (4), 043513.
- CONWAY, G.D., SMOLYAKOV, A.I. & IDO, T. 2021 Geodesic acoustic modes in magnetic confinement devices. *Nucl. Fusion* **62** (1), 013001.
- HEIDBRINK, W.W., VAN ZEELAND, M.A., AUSTIN, M.E., BIERWAGE, A., CHEN, L., CHOI, G.J., LAUBER, P., LIN, Z., MCKEE, G.R. & SPONG, D.A. 2020 ‘BAAE’ instabilities observed without fast ion drive. *Nucl. Fusion* **61** (1), 016029.
- KENNEDY, D., GIACOMIN, M., CASSON, F. J., DICKINSON, D., HORNSBY, W. A., PATEL, B. S. & ROACH, C. M. 2023 Electromagnetic gyrokinetic instabilities in the Spherical Tokamak for Energy Production (STEP) part II: transport and turbulence. Preprint, arXiv:2307.01669.
- KOLMES, E.J., OCHS, I.E. & FISCH, N.J. 2022 Wave-supported hybrid fast-thermal p-11B fusion. *Phys. Plasmas* **29** (11), 110701.
- LESUR, M., DIAMOND, P.H. & KOSUGA, Y. 2014 Nonlinear current-driven ion-acoustic instability driven by phase-space structures. *Plasma Phys. Control. Fusion* **56** (7), 075005.
- LI, H.Y., LI, S.J., XIE, Q.F., LIU, J.H., BAI, R.H., TAO, R.Y. & DENG, B.H. 2022b Thomson scattering diagnostic system for the XuanLong-50 experiment. *Rev. Sci. Instrum.* **93** (5), 053504.
- LI, S.J., BAI, R.H., TAO, R.Y., LI, N., LUN, X.C., LIU, L.C., LIU, Y., LIU, M.S. & DENG, B.H. 2021 A quasi-optical microwave interferometer for the XuanLong-50 experiment. *J. Instrum.* **16**, T08011.
- MA, R., HEIDBRINK, W.W., CHEN, L., ZONCA, F. & QIU, Z. 2023 Low-frequency shear Alfvén waves at DIII-D, theoretical interpretation of experimental observations. *Phys. Plasmas* **30** (4), 042105.
- SHI, Y. et al. 2022 Solenoid-free current drive via ECRH in EXL-50 spherical torus plasmas. *Nucl. Fusion* **62** (8), 086047.
- SPONG, D.A., HEIDBRINK, W.W., PAZ-SOLDAN, C., DU, X.D., THOME, K.E., VAN ZEELAND, M.A., COLLINS, C., LVOVSKIY, A., MOYER, R.A., AUSTIN, M.E., BRENNAN, D.P., LIU, C., JAEGER, E. F. & LAU, C. 2018 First direct observation of runaway-electron-driven whistler waves in tokamaks. *Phys. Rev. Lett.* **120** (15), 155002.
- TERRY, P.W. 2000 Suppression of turbulence and transport by sheared flow. *Rev. Mod. Phys.* **72** (1), 109.
- WANG, M., et al. 2023a Experimental investigation of kinetic instabilities driven by runaway electrons in the EXL-50 spherical torus. Preprint, arXiv:2307.06498.
- WANG, M., CHENG, S.K., LIU, B., SONG, S.D., GOU, D., SONG, Y.Y., LIU, W.J., BANERJEE, D., LI, S.J., SUN, T., GU, X., LI, Y., DONG, J., SHI, Y., PENG, Y.-K.M. & LIU, A. 2023b Generation of energetic electrons by an electron cyclotron wave through stochastic heating in a spherical tokamak. *J. Plasma Phys.* **89** (6), 905890603.
- WANG, M., LI, J., BAI, Y., DONG, J., SHI, Y., ZOU, X. & ENN TEAM. 2023c Particle pump-out induced by trapped electron mode turbulence in electron cyclotron heated plasmas on XuanLong-50 spherical torus. *Nucl. Fusion* **63** (7), 076024.
- WANG, M., LUN, X., BO, X., LIU, B., LIU, A. & SHI, Y. 2023d Radio-frequency measurements of energetic-electron-driven emissions using high-frequency magnetic probe on XuanLong-50 spherical torus. *Plasma Sci. Technol.* **25** (4), 045104.
- WANG, M., SHI, Y.J., DONG, J.Q., GAO, X.L., LU, Q.M., WANG, Z.Q., CHEN, W., LIU, A., ZHUANG, G., WANG, Y.M., et al. 2024 Low-frequency whistler waves driven by energetic electrons in plasmas of solely electron cyclotron wave heating. *Phys. Plasmas* **31** (3), 032105.
- ZONCA, F., CHEN, L. & SANTORO, R.A. 1996 Kinetic theory of low-frequency Alfvén modes in tokamaks. *Plasma Phys. Control. Fusion* **38** (11), 2011–2028.